Hindawi
International Journal of Optics
Volume 2024, Article ID 6658471, 10 pages
https://doi.org/10.1155/2024/6658471

Research Article

Dual Optical Injection in Semiconductor Lasers with Zero Henry Factor

Najm M. Al-Hosiny

Department of Physics, College of Science, Taif University, P.O. Box 1109, Taif 21944, Saudi Arabia

Correspondence should be addressed to Najm M. Al-Hosiny; nalhosiny@yahoo.co.uk

Received 13 February 2024; Revised 18 April 2024; Accepted 27 April 2024; Published 7 May 2024

Academic Editor: Sulaiman W. Harun

The dynamics of semiconductor lasers subject to dual optical injections are numerically investigated with a zero linewidth enhancement factor. With the aid of stability maps, we show that different chaotic and nonlinear dynamics can be produced (even with zero linewidth enhancement factor) by injecting an additional optical signal. We also study the bifurcation of the system and the carrier dynamics under dual optical injection and a zero linewidth enhancement factor.

1. Introduction

Optically injected semiconductor lasers have recently gained huge attention due to their chaotic behavior, which can be utilized in many telecommunication applications [1]. Injecting more than one signal has shown to be a very effective technique to enhance and control chaos in semiconductor lasers [2–4]. It has also shown to enrich the nonlinear dynamics and introduce different chaotic scenarios [5, 6]. It was also used to stabilize self-mode-locked QDash lasers along with optical feedback [7]. Recently, optical injection and optical feedback have been used to produce a reservoir computing system with a good (numerically predicted) performance [8]. Chaotic synchronization has also been achieved in mutually [9] unidirectionally coupled injected semiconductor lasers [10]. Li and others have recently managed to use chaos in semiconductor lasers in image encoding and decoding [11]. Optical frequency comb has also been generated [12] and injected [13] in semiconductor lasers. Qi and Lui have shown that the injection of dual beams can result in different scenarios in terms of the dominance of one of the two injected signals and identified the resultant chaotic behaviors in each scenario [14].

We have previously shown the carrier dynamics in semiconductor lasers under dual optical injection [15, 16]. We have also shown that the additional injected signal can be used to control routes to chaos in optically injected semiconductor lasers [17]. Finally, and very recently, we have drawn 3D maps of the dynamics of semiconductor lasers under multiple optical injections [18].

One of the most important features of semiconductor lasers as class B lasers is the linewidth enhancement factor (LEF) or Henry factor, which is believed to be responsible for many dynamics including chaos [19–21]. Therefore, many methods have been proposed to measure [22–24] and manipulate [25] this factor. Vazquez and others have reported the increase of this factor with increasing carrier density and decreasing temperature and energy level separation [26]. However, the most astonishing results are the reporting of zero [27] and negative LEF [28, 29]. We have previously shown that this factor plays a major role in forming the stability map and hence the chaotic behavior in optically injected semiconductor lasers [30]. We have also found this factor to be a good tool to control routes to chaos in optically injected semiconductor lasers [31].

It should be noted that the external optical injection technique provides more controllability compared to optical

feedback. That is mainly because that the laser in this case is perturbed with an independent external optical field (not self-feedback), which provides direct information about the laser cavity and gain medium.

In this paper, we raise a simple question, can the additional injected signal produce chaos and nonlinear dynamics in semiconductor lasers even if the LEF value was reduced to zero? To our knowledge, this was not investigated before. We numerically examined that by generating the stability map and studying the bifurcation of the system as well as the carrier density dynamics.

2. Materials and Methods

The model used in this study is based on Lang's approach [32]. The model consists of three semiconductor lasers. The first one is the laser being injected, which is called the slave laser (SL), and the other tunable lasers, which are injected into the SL, are called master lasers (ML_1 and ML_2). The schematic diagram of this model is shown in Scheme 1.

The rate equations of the system can be expressed as follows:

$$\frac{d}{dt}E_o(t) = \frac{1}{2}G_N\Delta N(t)E_o(t) + \eta\left[E_1\cos(\Delta t_1) + E_2\cos(\Delta t_2)\right], \tag{1}$$

$$\frac{d}{dt}\varphi_o(t) = \frac{1}{2}\alpha G_N\Delta N(t) + \eta\left[\frac{E_1}{E_o(t)}\sin(\Delta t_1) + \frac{E_2}{E_o(t)}\sin(\Delta t_2)\right], \tag{2}$$

$$\frac{d}{dt}N(t) = J - \frac{N(t)}{\tau_s} - G_N\left(N(t) - N_o\right)E_o^2(t), \tag{3}$$

where $E_o(t)$, E_1 and E_2 are the electric field of the SL and $ML_{1,2}$, respectively, $\Delta N(t)$ is the population inversion, which is defined as $N - N_{th}$ where N is the carrier density and N_{th} is its value at threshold, G_N is the material gain coefficient, η is the coupling term, $\Delta t_m = \Delta\omega_m t - \varphi_o(t)$, where $\Delta\omega_m = \omega_m - \omega_o$ (the angular frequency detuning between the SL laser and the $ML_{1,2}$), $\varphi_o(t)$ is the phase of the SL, α is the Henry factor or the linewidth enhancement factor, and N_o is the carrier density at transparency. τ_s is the lifetime for spontaneous emission and nonradiative recombination, and J is the injected current density. The main variables of the system are the frequency detuning (Δf) and the injection level (K). Δf corresponds to, while K is the ratio of the injected field ($E_{1,2}$) to the free running SL field (E_{os}), which is given by $E_{os} = \sqrt{\tau_p(J - N_{th}/\tau_s)}$, where τ_p is the photon lifetime. The rate equations are numerically integrated (using Runge–Kutta method) to identify the bifurcation of the system and draw the stability maps (the dynamics of the SL in the plane of Δf vs K) and also to calculate the normalized carrier density (the ratio of the carriers of the system to the threshold carriers). The power spectra are generated by applying FFT to a chosen window of the SL electric field time window. Finally, it should be noted that all the parameters used here are based on experimental characterization [33] and are listed in Table 1. Finally, this model is suitable for the distributed feedback laser (DFB) and should be modified when used for other types of semiconductor lasers as other phenomena should be considered as the polarization in vertical cavity surface emitting lasers (VCSELs).

3. Results and Discussion

In order to study the effect of the additional injected signal in the case of zero LEF, we first draw the stability map of the system under the injection of one signal and with zero LEF as shown in Figure 1. The clear white region represents the locking area, where the SL is stably locked to the ML. The stability here is defined as the side peaks do not exceed −50 dB compared to the free-running SL [33].

The grey colors indicate the quasiperiodic behavior (the darker the grey means more periodicity), while the black regions represent the chaotic behaviors. The first feature that can be noticed is the shrinkage of the chaotic regions compared to that in the case of nonzero LEF [2]. Another expected feature of the map is the symmetry as the nonzero value of the LEF was previously reported to be responsible for the asymmetry in the stability map [33]. This symmetry here is not only shown in the locking region but also all over the map.

Now, we inject the second signal (ML_2) at three different operating points (a, b, and c) as marked in Figure 1. In other words, we inject the second signal in three different regions: the period-one region (a), the stable locking (b), and the quasiperiodic region (c). The first operating point (a) at $K_2 = 0.1$ and $\Delta f_2 = +7.5$ GHz, where the SL is not locked to ML_1, but showing period-one behavior. When injecting the ML_2 at this point, the stability map changes and the resultant stability map is shown in Figure 2. It can be seen that the locking bandwidth maintained its shape and characteristics. However, most of this region is covered by the grey color, where the SL is unstably locked to ML_1 with the strong presence of ML_2. This region is sometimes referred to as self-pulsation [34], where the side peaks and the second injected signal oscillate around the relaxation oscillation frequency (ROF). Such behavior (at label a in Figure 2) is shown in Figure 3(a), which is illustrated in three columns, the power spectra as a function of frequency detuning, the SL electric field time series, and the projection of the electric field (E) and the carrier density (n).

The SL is locked to ML_1 with a strong presence of ML_2. The self-pulsation (or period-one) behavior is clearly shown

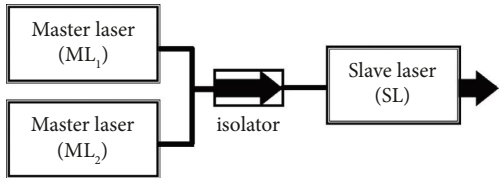

Scheme 1: The schematic diagram of our model.

Table 1: Parameters used in our simulation as experimentally characterized.

Parameter	Symbol	Value
Wavelength	λ	1556.6 nm
Differential gain	G_N	$1.4\times10^{-12}\,\mathrm{m^3\cdot s^{-1}}$
Carrier lifetime	τ_s	0.43 ns
Photon lifetime	τ_p	1.8 ps
Coupling rate	η	$9\times10^{10}\,\mathrm{s^{-1}}$
Transparency carrier density	N_o	$1.1\times10^{24}\,\mathrm{m^{-3}}$
Threshold carrier density	N_{th}	$1.5\times10^{24}\,\mathrm{m^{-3}}$
Normalized injection current	I/I_{th}	2

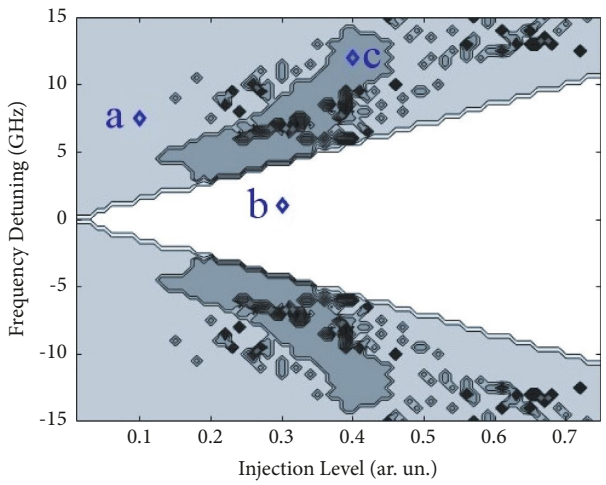

Figure 1: Stability map of the system under a single optical injected signal and with a zero LEF. The labels (a, b, and c) represent the operation points where the second signal (ML_2) is injected as will be discussed later (remember that ML_2 in all cases is injected at $K_2 = 0.1$ and $\Delta f_2 = +7.5$).

in electric field time series and its projection with carriers. As shown in the map, the stable locking region (i.e. clear white) seems to be confined in a narrow band around ML_2 (+7.5 GHz). Inside this region, the SL is stably locked to ML_1 with suppressed ML_2 as shown in Figure 3(b) and denoted in Figure 2 by label (b).

The white grey line shown around +7.5 GHz is resulting from the presence of ML_2. Even when the system exhibits chaotic behaviors in the positive detuning side, at this point (+7.5 GHz), the system shows self-pulsation behavior as shown in Figure 3(c) and denoted in Figure 2 by label (c). On the other hand, the chaotic dynamics (black color) seem to spread all over the map (outside the locking bandwidth),

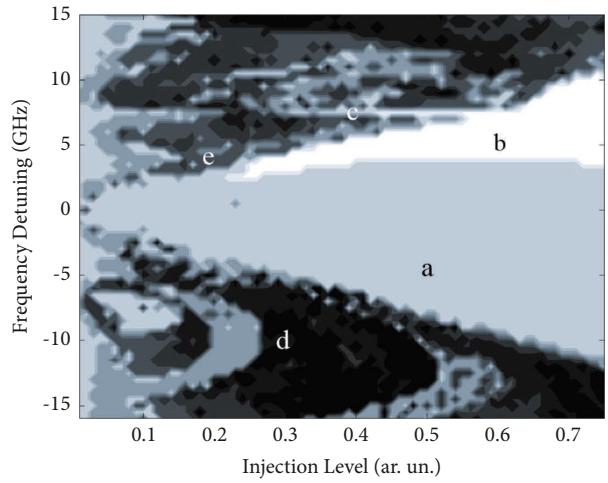

Figure 2: Stability map of the system under dual optical injected signals and with a zero LEF. ML_2 is injected at $K_2 = 0.1$ and $\Delta f_2 = +7.5$ GHz (label (a) in Figure 1). The labels (a to e) correspond to the points where the spectra in Figure 3 are taken.

especially at a higher injection level. A typical example of this behavior is taken at label (d) in Figure 2 and shown in Figure 3(d). The SL is not locked at all and largely depleted with the other side peaks. The final behavior observed in the map is the strong quasiperiodic dynamics, which is indicated by darker grey. Such behavior is taken at label (e) in Figure 2 and shown in Figure 3(e). The periodicity can easily be recognized in the E vs. n projection.

To further investigate the dynamics of the system, we generate bifurcation diagram by recording the extrema of E as a function of frequency detuning at a constant injection level as shown in Figures 4(a) and 4(b). As shown in the figure, the behaviors mentioned before are clearly evident with different possible routes to chaos (i.e., quasiperiodic route). Moreover, the self-pulsation dynamic is also shown inside the locking bandwidth. The corresponding dynamics of carriers are shown in Figures 4(c) and 4(d). The variation of carriers increases largely inside the locking bandwidth and obviously depending on the injection level and takes its maximum value at the free running SL frequency. The spikes shown in Figure 4(d) at +7.5 GHz correspond to ML_2 as it causes a hole burning in the carrier spectra when both MLs coincides. This spike is not shown in Figure 4(c) as ML_2 in this case is outside the locking bandwidth and the injection level is also lower than in (d).

The second case of injection is injecting ML_2 inside the stable locking region at label (b) shown in Figure 1. The resultant stability map in this case is shown in Figure 5. It can be seen from the figure that the chaotic dynamics disappeared completely as the SL is stably locked to ML_2. The new stable locking region largely shrinks and shifts up around ML_2 (at +1 GHz). Such behavior of stable locking is taken at label (a) in Figure 5 and shown in Figure 6(a). The two islands of the quasiperiodic behavior (dark grey) shown in the original map are still evident in the resultant map and in both sides of detuning. A typical example of this behavior is taken at point (b) in Figure 5 and shown in Figure 6(b).

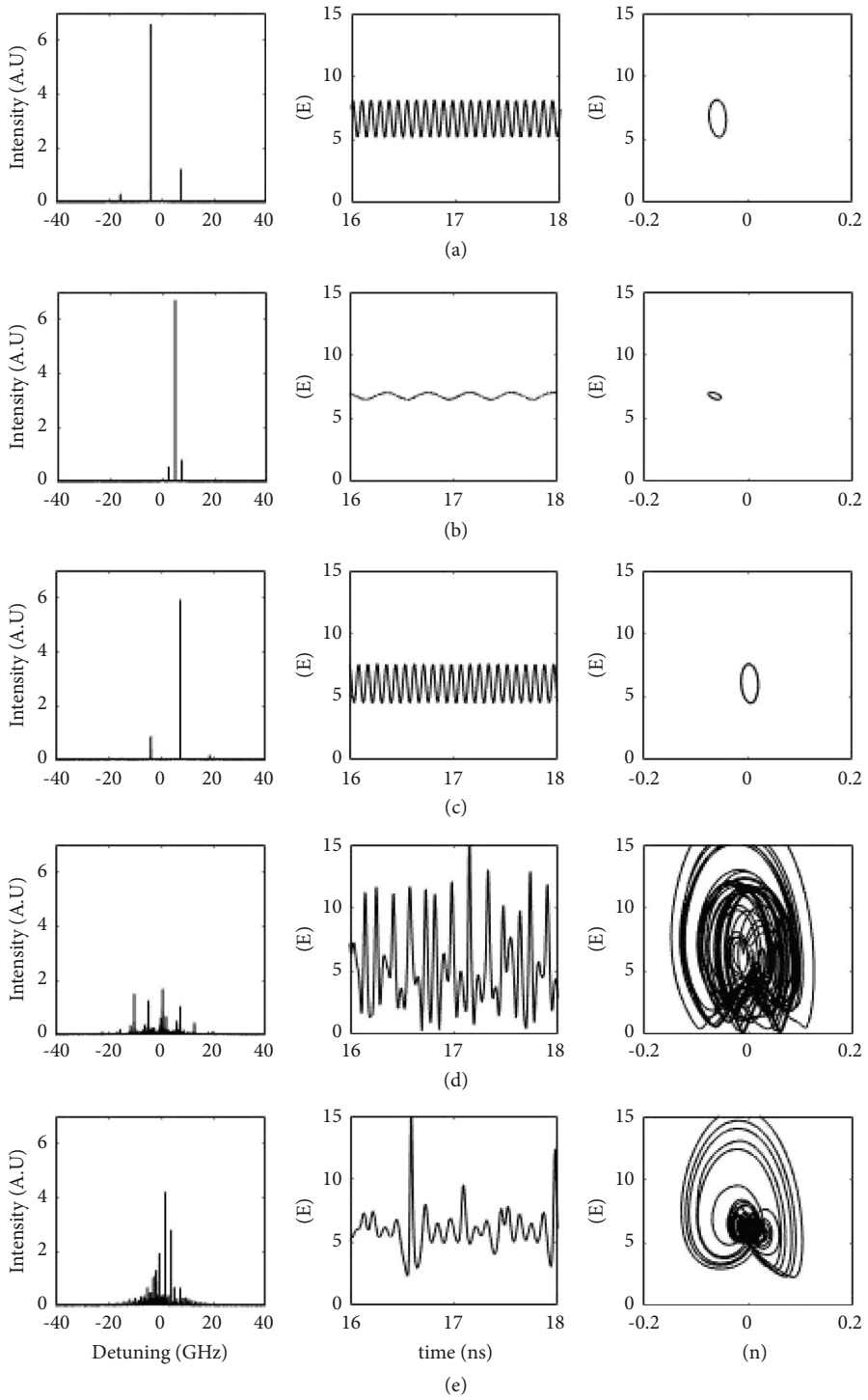

FIGURE 3: Power spectra (1st column), electric field time series (2nd column), and the projection of electric field (E) and carrier densities (n) (3rd column). The operating points at which these spectra are taken (a-e) are shown in Figure 2.

The rest of the map is covered by period-one behavior (light grey) as shown at point (c) in the figure and illustrated in Figure 6(c).

The bifurcation diagrams of this stability map in this case are shown in Figure 7. The period one and quasiperiodic dynamics are clearly shown with no chaotic dynamics. The variation of carriers is confined in a narrow band due to the locking bandwidth itself and again is dependent on the injection level with no unexpected features.

Finally, we inject ML_2 inside the quasiperiodic region at label (c) in Figure 1. The resulting stability map is shown in Figure 8.

The first notice that can be observed here is the disappearance of the stable locking region (white color) as ML_2 is

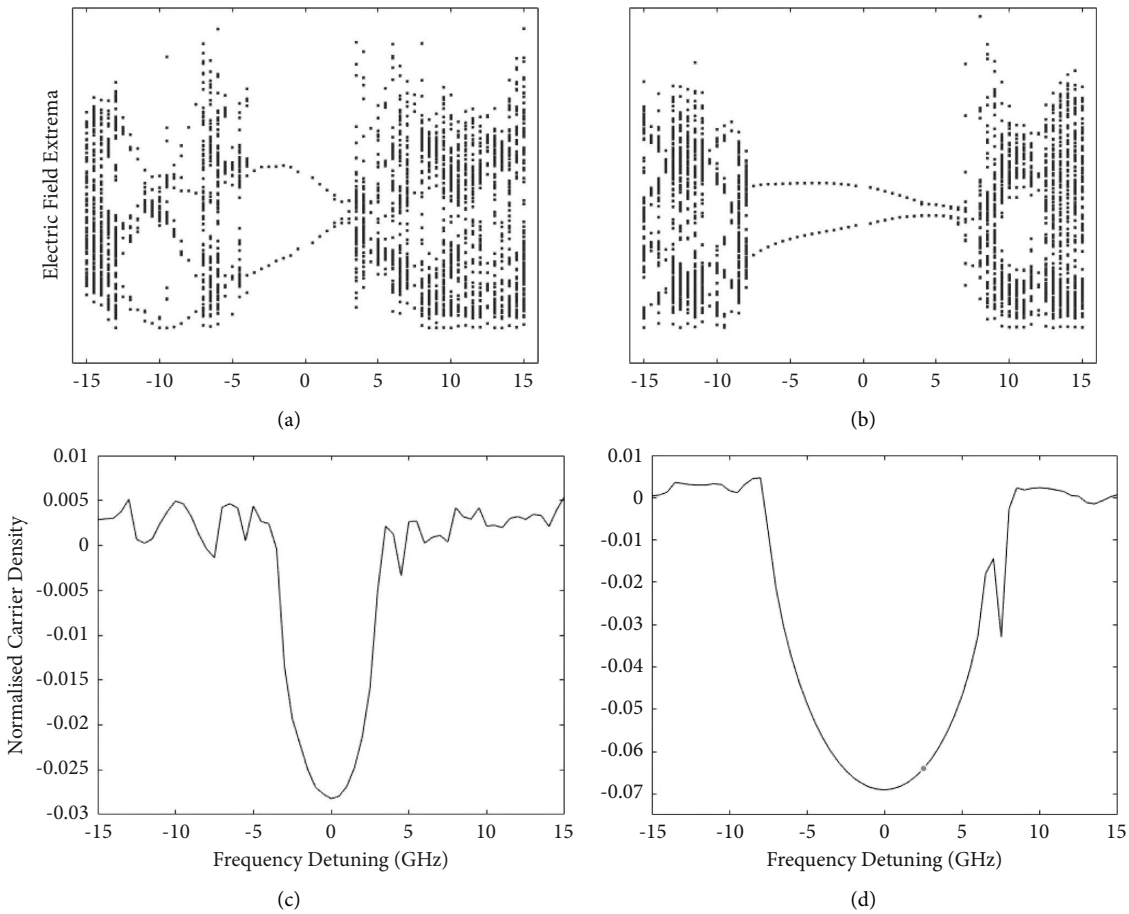

FIGURE 4: Bifurcation diagrams of the stability map are shown in Figure 2 at (a) $K_1 = 0.2$ and (b) $K_1 = 0.5$. (c, d) illustrate the corresponding carriers' dynamics.

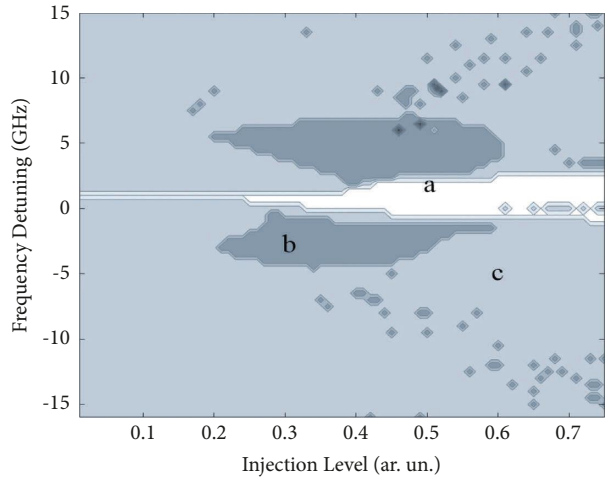

FIGURE 5: Stability map of the system under dual optical injected signals and with a zero LEF. ML_2 is injected at $K_2 = 0.3$ and $\Delta f_2 = 1$ GHz (label (b) in Figure 1).

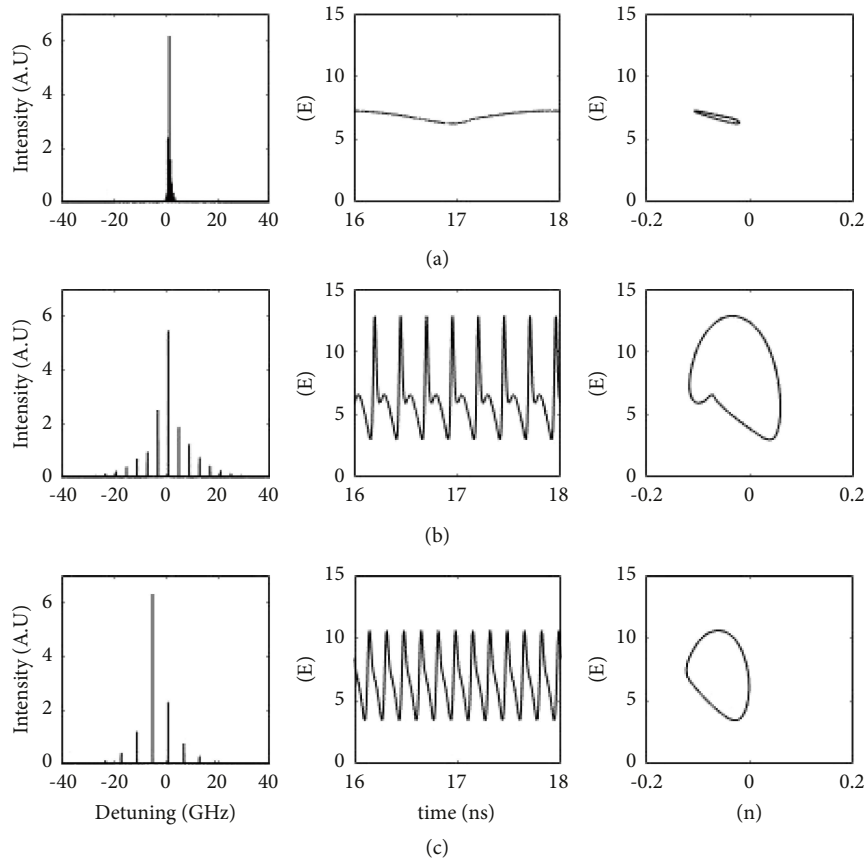

Figure 6: Power spectra (1st column), electric field time series (2nd column), and the projection of electric field (E) and carrier densities (n) (3rd column). The operating points at which these spectra are taken (a-c) are shown in Figure 5.

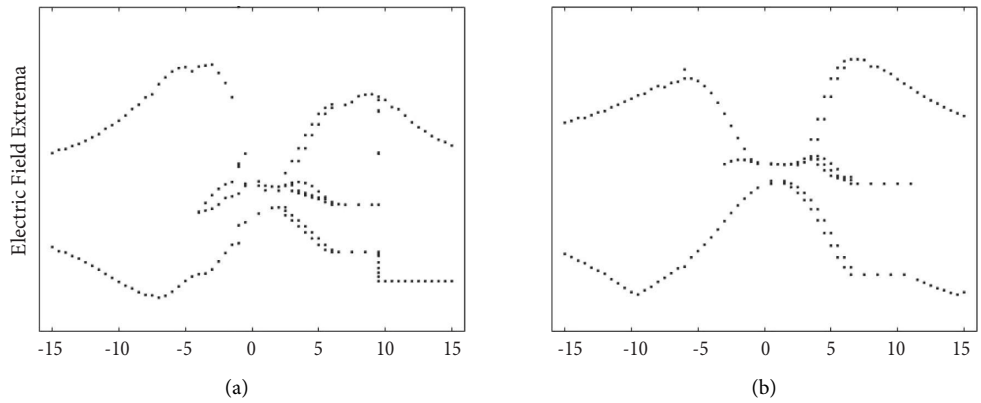

Figure 7: Continued.

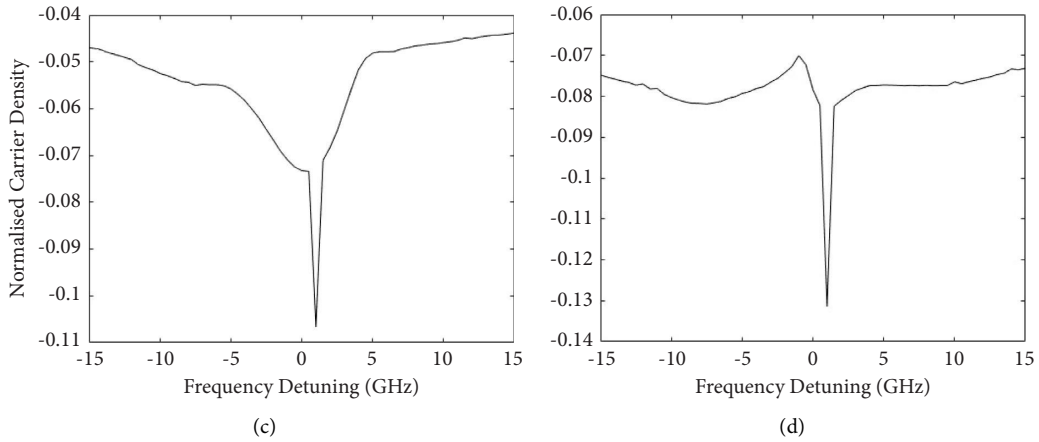

Figure 7: Bifurcation diagrams of the stability map are shown in Figure 5 at (a) $K_1 = 0.3$ and (b) $K_1 = 0.5$. (c, d) illustrate the corresponding carriers' dynamics.

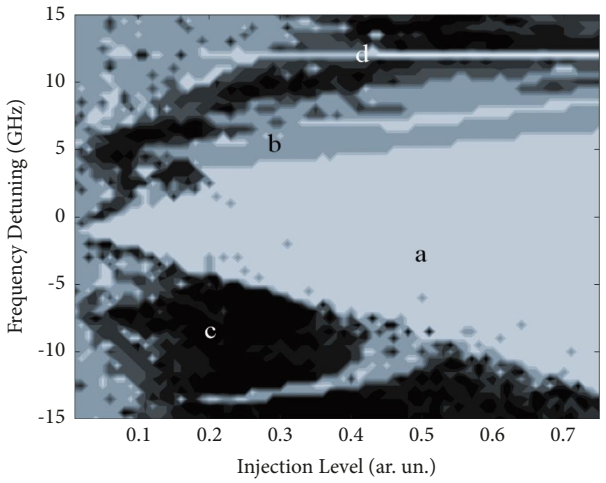

Figure 8: Stability map of the system under dual optical injected signals and with a zero LEF. ML_2 is injected at $K_2 = 0.4$ and $\Delta f_2 = 12$ GHz (label (c) in Figure 1).

injected far away from this region. The general features of the self-pulsation region (light grey) are still evident with some distortion in the positive detuning side (where ML_2 is injected). This behavior is taken at label (a) in Figure 8 and shown in Figure 9(a). A clear period-one or self-pulsation is shown.

The quasiperiodic behavior (dark grey) is observed in a large stripe at the top of the locking bandwidth and also in a large area in the positive detuning side. An example of this behavior is taken at label (b) in this figure and shown in Figure 9(b). The quasiperiodic dynamic is clearly shown in the electric field time series and in the projection of E and n. The chaotic dynamics (black color) in this case are also evident covering the rest of the map, especially at the negative detuning side. Such behavior is taken at label (c) in the Figure and shown in Figure 9(c). Finally, when both MLs coincide (at +12 GHz), the resulting behavior is period-one as shown by the light grey line and the behavior is illustrated in Figure 9(d).

The bifurcation diagrams of this map are shown in Figure 10. Various routes to chaos can be spotted in the diagrams, while inside the locking bandwidth, the system always maintains self-pulsation dynamics as previously mentioned. The dynamics of carriers exhibit the same characteristics discussed before with holes burning at ML_2 (at +12 GHz) or around the ROF (around 5 GHz). The variation also increases with a higher injection level.

Finally, we should mention that this model has shown very good agreement with experimental results in terms of tailoring enhanced chaos in optically injected semiconductor lasers [2] and is trusted to give good agreement with reality in this case.

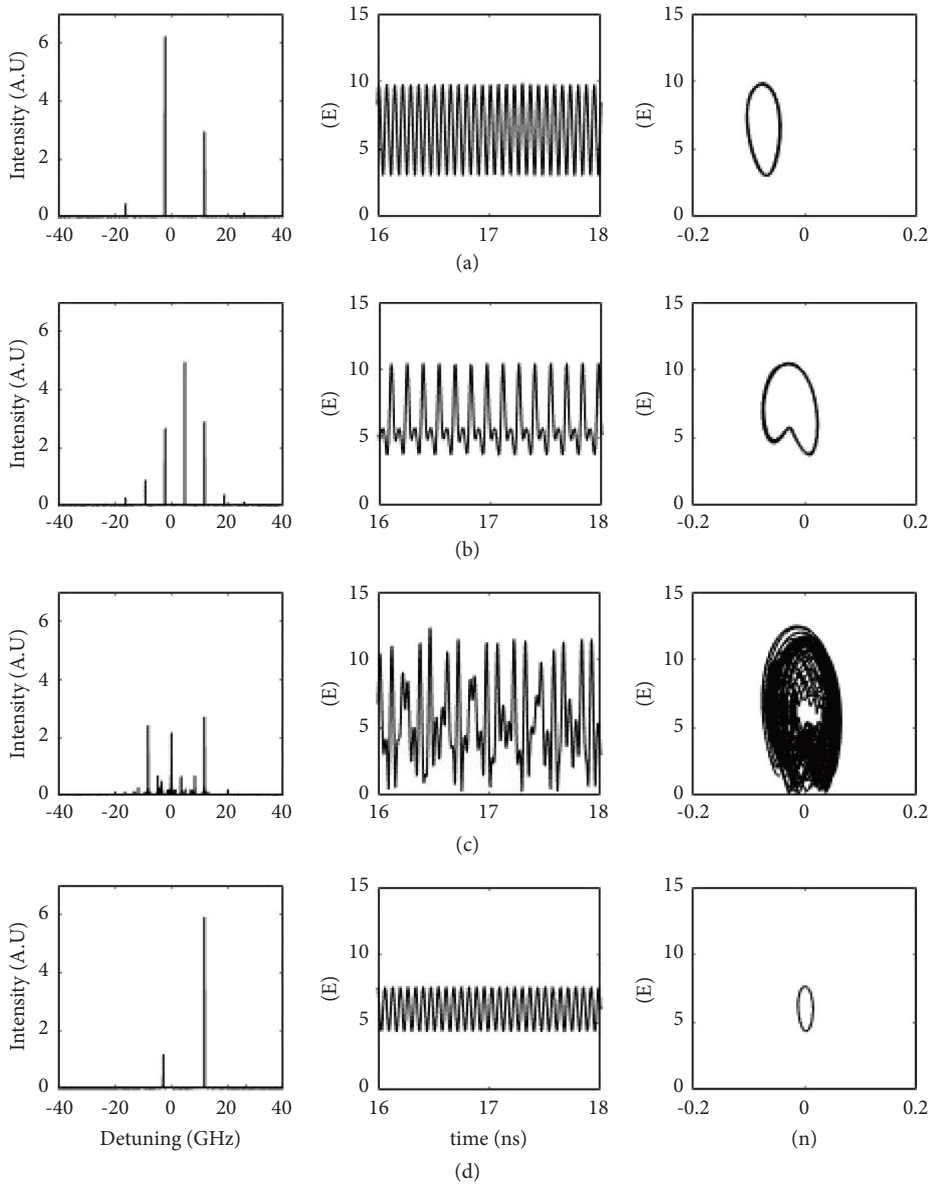

Figure 9: Power spectra (1st column), electric field time series (2nd column), and the projection of electric field (E) and carrier densities (n) (3rd column). The operating points at which these spectra are taken (a-d) are shown in Figure 8.

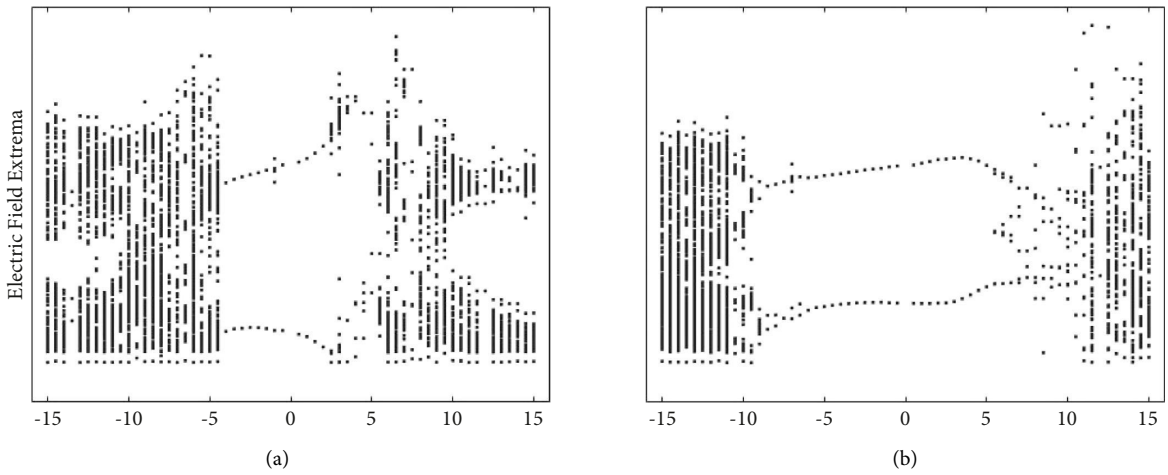

Figure 10: Continued.

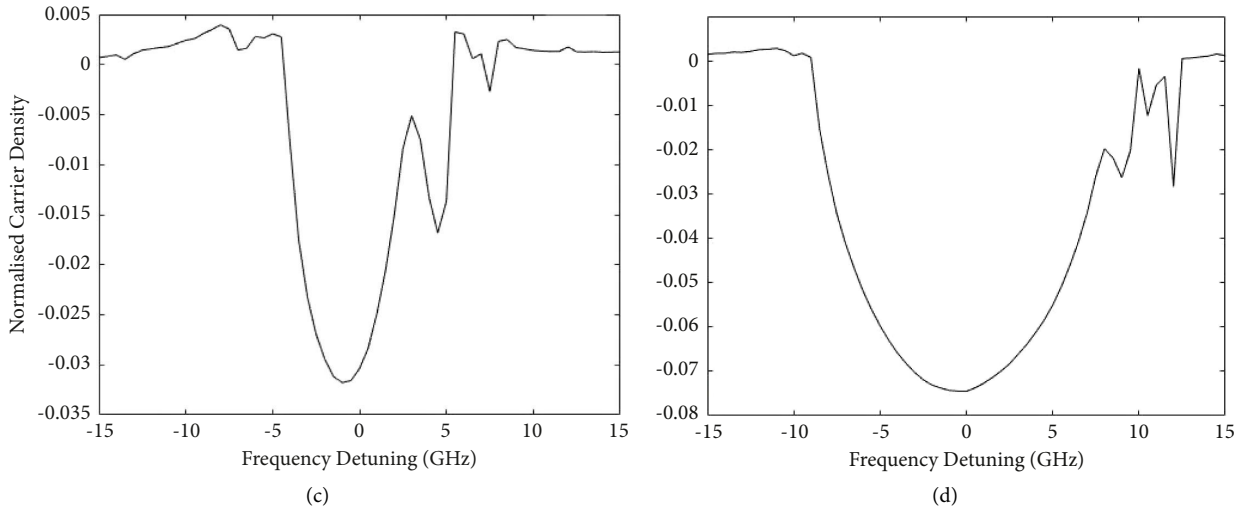

FIGURE 10: Bifurcation diagrams of the stability map are shown in Figure 8 at (a) $K_1 = 0.2$ and (b) $K_1 = 0.5$. (c, d) illustrate the corresponding carriers' dynamics.

4. Conclusions

Dual optical injection dynamics in semiconductor lasers are numerically investigated when the LEF is reduced to zero. Despite the fact that the LEF plays a major rule in producing rich nonlinear and chaotic dynamics, the injection of an additional signal has shown to produce such behaviors even with a zero LEF. The stability maps in all cases seem to be symmetrical in terms of locking bandwidth. However, chaotic and nonlinear dynamics solely depend on the operating points at which the additional signal is injected. Further experimental investigation could clarify the theoretical expectation, which could be the next step to take.

These results are believed to be very advantageous in many modern telecommunication applications where the chaos and nonlinear dynamics are desirable (such as in cryptographical communication) when using lasers with very low LEF as in the case of quantum dot lasers [35, 36].

Data Availability

The data supporting the findings of this study are included in the article.

Conflicts of Interest

The authors declare that they have no conflicts of interest.

Acknowledgments

The researcher would like to acknowledge Taif University for funding this work.

References

[1] J. Liu, H. Chen, and S. Tang, "Optical-communication systems based on chaos in semiconductor lasers," *IEEE Transactions on Circuits and Systems I: Fundamental Theory and Applications*, vol. 48, pp. 1475–1483, 2001.

[2] N. M. Al-Hosiny, I. D. Henning, and M. J. Adams, "Tailoring enhanced chaos in optically injected semiconductor lasers," *Optics Communications*, vol. 269, no. 1, pp. 166–173, 2007.

[3] H. Han, M. J. Zhang, and K. A. Shore, "Chaos bandwidth enhancement of Fabry–Pérot laser diode with dual-mode continuous-wave optical injection," *IEEE Journal of Quantum Electronics*, vol. 55, no. 3, pp. 1–8, 2019.

[4] Y. Zeng, P. Zhou, Y. Huang, and N. Li, "Optical chaos generated in semiconductor lasers with intensity-modulated optical injection: a numerical study," *Applied Optics*, vol. 60, no. 26, pp. 7963–7972, 2021.

[5] M. AlMulla, X.-Q. Qi, and J.-M. Liu, "Dynamics maps and scenario transitions for a semiconductor laser subject to dual-beam optical injection," *IEEE Journal of Selected Topics in Quantum Electronics*, vol. 19, no. 4, p. 1501108, 2013.

[6] A. A. Hemed and R. S. Abbas, "Enhanced emission perturbations associated with mixed optical injection in laser diode," *AIP Conference Proceedings*, 2020.

[7] H. Asghar, E. Sooudi, and J. G. McInerney, "Stabilization of self-mode-locked QDash lasers subject to simultaneous continuous-wave optical injection and optical feedback," *Applied Optics*, vol. 57, no. 22, pp. E45–E49, 2018.

[8] Y. Hou, G. Xia, W. Yang et al., "Prediction performance of reservoir computing system based on a semiconductor laser subject to double optical feedback and optical injection," *Optics Express*, vol. 26, no. 8, pp. 10211–10219, 2018.

[9] Y. Senlin, "Chaotic synchronization of mutually coupled lasers with another laser and its encoding application in secret communication," *Journal of Optical Communications*, vol. 44, no. s1, pp. s673–s682, 2020.

[10] H. A. Hammood and H. Sultan, "Chaotic synchronization of unidirectionally coupled multimode semiconductor laser," *AIP Conference Proceedings*, 2020.

[11] X. Li, B. Li, B. Sun, Z. Wang, C. Wang, and J. Mou, "A new image encryption algorithm based on modified optically injected semiconductor laser chaotic system," *IEEE Access*, vol. 9, pp. 131542–131551, 2021.

[12] Y. Doumbia, T. Malica, D. Wolfersberger, K. Panajotov, and M. Sciamanna, "Nonlinear dynamics of a laser diode with an injection of an optical frequency comb," *Optics Express*, vol. 28, no. 21, pp. 30379–30390, 2020.

[13] K. Yang, Y. Zhang, S. Liao et al., "Optical frequency comb generation by mutual injection in twin-stripe semiconductor laser," *Semiconductor Lasers and Applications XI*, pp. 120–126, 2021.

[14] X.-Q. Qi and J.-M. Liu, "Dynamics scenarios of dual-beam optically injected semiconductor lasers," *IEEE Journal of Quantum Electronics*, vol. 47, no. 6, pp. 762–769, 2011.

[15] N. Al-Hosiny, "Electron density variation in optically injected semiconductor lasers," *FEJE*, vol. 2, pp. 57–64, 2008.

[16] N. M. Al-Hosiny, "Electron density dynamics in semiconductor lasers under relatively strong dual optical injection," *Optics Communications*, vol. 281, no. 17, pp. 4488–4492, 2008.

[17] N. M. Al-Hosiny, "Sensitivity of routes to chaos in optically injected semiconductor lasers," *Journal of Nonlinear Optical Physics and Materials*, vol. 23, no. 03, p. 1450036, Article ID 1450036, 2014.

[18] N. M. Al-Hosiny, "3D Injection-locking maps of semiconductor laser under multiple optical injections," *Journal of Optics*, vol. 50, no. 4, pp. 629–636, 2021.

[19] C. Henry, "Theory of the linewidth of semiconductor lasers," *IEEE Journal of Quantum Electronics*, vol. 18, no. 2, pp. 259–264, 1982.

[20] M. Osinski and J. Buus, "Linewidth broadening factor in semiconductor lasers--An overview," *IEEE Journal of Quantum Electronics*, vol. 23, no. 1, pp. 9–29, 1987.

[21] G. P. Agrawal and C. M. Bowden, "Concept of linewidth enhancement factor in semiconductor lasers: its usefulness and limitations," *IEEE Photonics Technology Letters*, vol. 5, no. 6, pp. 640–642, 1993.

[22] Y. Yu, G. Giuliani, and S. Donati, "Measurement of the linewidth enhancement factor of semiconductor lasers based on the optical feedback self-mixing effect," *IEEE Photonics Technology Letters*, vol. 16, no. 4, pp. 990–992, 2004.

[23] G. Giuliani, S. Donati, and W. Elsässer, "Measurement of linewidth enhancement factor of different semiconductor lasers in operating conditions," *SPIE Proceedings*, pp. 416–424, 2006.

[24] Y. Fan, Y. Yu, J. Xi, G. Rajan, Q. Guo, and J. Tong, "Simple method for measuring the linewidth enhancement factor of semiconductor lasers," *Applied Optics*, vol. 54, no. 34, pp. 10295–10298, 2015.

[25] N. Naderi, M. Pochet, F. Grillot, A. Shirkhorshidian, V. Kovanis, and L. Lester, "Manipulation of the linewidth enhancement factor in an injection-locked Quantum-Dash Fabry-Perot laser at 1550nm," in *Proceedings of the 2010 23rd Annual Meeting of the IEEE Photonics Society*, pp. 427-428, Denver, CO, USA, November 2010.

[26] J. Vazquez, H. Nilsson, J.-Z. Zhang, and I. Galbraith, "Linewidth enhancement factor of quantum-dot optical amplifiers," *IEEE Journal of Quantum Electronics*, vol. 42, no. 10, pp. 986–993, 2006.

[27] P. K. Kondratko, S.-L. Chuang, G. Walter, T. Chung, and N. Holonyak, "Observations of near-zero linewidth enhancement factor in a quantum-well coupled quantum-dot laser," *Applied Physics Letters*, vol. 83, no. 23, pp. 4818–4820, 2003.

[28] R. R. Alexander, D. Childs, H. Agarwal et al., "Zero and controllable linewidth enhancement factor in p-doped 1.3 μm quantum dot lasers," *Japanese Journal of Applied Physics*, vol. 46, no. 4S, p. 2421, 2007.

[29] M. Pereira, "The linewidth enhancement factor of intersubband lasers: from a two-level limit to gain without inversion conditions," *Applied Physics Letters*, vol. 109, no. 22, 2016.

[30] N. M. Al-Hosiny, "Effect of linewidth enhancement factor on the stability map of optically injected distributed feedback laser," *Optical Review*, vol. 21, no. 3, pp. 261–264, 2014.

[31] N. Al-Hosiny, "Effect of linewidth enhancement factor (LEF) on routes to chaos in optically injected semiconductor lasers," *Optica Applicata*, vol. 51, no. 4, pp. 621–632, 2021.

[32] R. Lang, "Injection locking properties of a semiconductor laser," *IEEE Journal of Quantum Electronics*, vol. 18, no. 6, pp. 976–983, 1982.

[33] N. M. Al-Hosiny, I. D. Henning, and M. J. Adams, "Correlation of electron density changes with optical frequency shifts in optically injected semiconductor lasers," *IEEE Journal of Quantum Electronics*, vol. 42, no. 6, pp. 570–580, 2006.

[34] C. Henry, N. Olsson, and N. Dutta, "Locking range and stability of injection locked 1.54 μm InGaAsp semiconductor lasers," *IEEE Journal of Quantum Electronics*, vol. 21, no. 8, pp. 1152–1156, 1985.

[35] K. Kobayashi, H. Nishimoto, and R. Lang, "Experimental observation of asymmetric detuning characteristics in semiconductor laser injection locking," *Electronics Letters*, vol. 18, pp. 54–56, 1982.

[36] L. Goldberg, H. Taylor, and J. Weller, "Locking bandwidth asymmetry in injection-locked GaAlAs lasers," *Electronics Letters*, vol. 18, pp. 986-987, 1982.